aerospace

MDPI

Article

Sensitivity Analysis of the Johnson-Cook Model for Ti-6Al-4V in Aeroengine Applications

Carlos Beecher [1,2], Héctor Sepúlveda [2,3], Angelo Oñate [4], Anne Marie Habraken [3,5], Laurent Duchêne [3], Gonzalo Pincheira [6] and Víctor Tuninetti [1,*]

1 Department of Mechanical Engineering, Universidad de La Frontera, Temuco 4811230, Chile; c.beecher01@ufromail.cl
2 Master Program in Engineering Sciences, Faculty of Engineering, Universidad de La Frontera, Temuco 4811230, Chile; hector.sepulveda@uliege.be
3 Department ArGEnCo-MSM, University of Liège, 4000 Liège, Belgium; anne.habraken@uliege.be (A.M.H.); l.duchene@uliege.be (L.D.)
4 Department of Materials Engineering (DIMAT), Faculty of Engineering, Universidad de Concepción, Concepción 4070415, Chile; aonates@udec.cl
5 F.R.S.—FNRS, Rue d'Egmont 5, 1000 Bruxelles, Belgium
6 Department of Industrial Technologies, University of Talca, Curicó 3340000, Chile; gpincheira@utalca.cl
* Correspondence: victor.tuninetti@ufrontera.cl

Abstract: Titanium alloys, such as Ti-6Al-4V, are crucial for aeroengine structural integrity, especially during high-energy events like turbine blade-out scenarios. However, accurately predicting their behavior under such conditions requires the precise calibration of constitutive models. This study presents a comprehensive sensitivity analysis of the Johnson-Cook plasticity and progressive damage model parameters for Ti-6Al-4V in blade containment simulations. Using finite element models, key plasticity parameters (yield strength (A), strain-hardening constant (B), strain-rate sensitivity (C), thermal softening coefficient (m), and strain-hardening exponent (n)) and damage-related parameters ($d1$, $d2$, $d3$, $d4$, and $d5$) were systematically varied by ±5% to assess their influence on stress distribution, plastic deformation, and damage indices. The results indicate that the thermal softening coefficient (m) and the strain rate hardening coefficient (C) exhibit the most significant influence on the predicted casing damage, highlighting the importance of accurately characterizing these parameters. Variations in yield strength (A) and strain hardening exponent (n) also notably affect stress distribution and plastic deformation. While the damage evolution parameters ($d1$–$d5$) influence the overall damage progression, their individual sensitivities vary, with $d1$ and $d4$ showing more pronounced effects compared to others. These findings provide crucial guidance for calibrating the Johnson-Cook model to enhance aeroengine structural integrity assessments.

Keywords: Johnson-Cook model; Ti-6Al-4V; titanium alloy; aeroengine; blade-out; sensitivity analysis; finite element analysis; structural integrity; damage tolerance; aircraft safety

Academic Editor: Xiang Zhang

Received: 29 November 2024
Revised: 18 December 2024
Accepted: 23 December 2024
Published: 24 December 2024

Citation: Beecher, C.; Sepúlveda, H.; Oñate, A.; Habraken, A.M.; Duchêne, L.; Pincheira, G.; Tuninetti, V. Sensitivity Analysis of the Johnson-Cook Model for Ti-6Al-4V in Aeroengine Applications. *Aerospace* **2025**, *12*, 3. https://doi.org/10.3390/aerospace12010003

1. Introduction

Titanium alloys, such as Ti-6Al-4V, are essential in aerospace engineering due to their exceptional strength-to-weight ratio, corrosion resistance, and high-temperature capabilities [1–7]. These alloys represent 14% of the total weight of modern aircraft [8], with critical components like blades, casings, and compressors requiring their use [9,10]. However, accurately modeling the complex deformation and damage behavior of titanium

alloys under the extreme conditions encountered in aeroengine applications remains a challenge [11–14].

The Johnson-Cook (J-C) plasticity and progressive damage model is widely used to simulate the high-strain-rate response of metallic materials [15–18], including titanium alloys [19–27]. This model accounts for the effects of strain, strain rate, stress triaxiality, and temperature on the material's strength, damage evolution, and fracture [22,28–30]. Accurate calibration of the Johnson-Cook model parameters is crucial for reliable predictions of the structural integrity of aeroengine components during high-energy events, such as turbine blade-out scenarios [5,31,32].

While aircraft engine technology has advanced [33–38], engine failures, particularly from fan or compressor blade detachment, remain a critical safety concern. Two key challenges necessitate an integrated approach for improved engine design: accurately modeling the initial blade impact on the casing and understanding the complex interplay between dynamic strength, resistance, and subsequent vibrations that contribute to further engine damage [39,40]. This study addresses the first challenge by focusing on the structural integrity of the casing during a blade-out event. Specifically, it performs a sensitivity analysis of the Johnson-Cook plasticity and progressive damage model for Ti-6Al-4V, a crucial titanium alloy used in aeroengine components. Accurately capturing the material response during impact is essential for predicting damage and ensuring containment, directly contributing to improved safety. Future research should integrate this impact model with a comprehensive vibration analysis to fully address the second challenge and enable a more accurate and robust engine design, ultimately minimizing the risk of catastrophic failure.

Despite the extensive use of the Johnson-Cook model [14,15], comprehensive sensitivity analyses focused on aerospace-grade titanium alloys, particularly in the context of turbofan structural integrity, are scarce [31,32,41–44]. Uncertainties in the model parameters can lead to inaccurate predictions that result in over-design, premature failure, or even compromise operational safety. This research gap highlights the urgent need for a detailed and rigorous sensitivity analysis of the Johnson-Cook plasticity and damage model for titanium alloys.

This study presents a comprehensive sensitivity analysis of the Johnson-Cook plasticity and progressive damage models for Ti-6Al-4V alloy to identify the most critical parameters influencing aeroengine component structural response. Using finite element simulations of a full low-pressure compressor blade-out event within a Trent 1000-based aeroengine, this work systematically evaluates key plasticity and damage model parameters, prioritizing the most influential parameters and quantifying their impact on fan blade containment predictions. This detailed analysis provides robust guidance for model calibration, leading to more reliable assessments of aeroengine structural integrity.

2. Materials and Methods

Sensitivity analysis quantifies the influence of input parameter variations on model outputs [45–47]. While uncertainty quantification is a broad concern across various fields, it is particularly critical in engineering complex systems with multiple uncertainty sources [48,49] affecting simulation results. This study employs a local sensitivity analysis [50], investigating the impact of $\pm 5\%$ variations in J-C plasticity and damage parameters on the predicted structural response. A local sensitivity analysis evaluates the influence of deterministic model parameters on the responses of interest [46].

The chemical composition and mechanical behavior of the titanium alloy Ti-6Al-4V has been previously characterized in Tuninetti et al. [51,52]. The J-C model parameters were previously calibrated for plasticity using artificial neural networks [30], while damage and

fracture were obtained through a combination of direct identification and finite element-based inverse calibration [22]. These parameters have been validated for temperatures between 25 °C and 400 °C and plastic strain rates up to 10^{-3} s^{-1}, ensuring their suitability for this study.

In explicit dynamics simulations, the Johnson-Cook model, incorporating plasticity, damage, and fracture, is a coupled constitutive framework where plastic deformation, damage evolution, and fracture are intrinsically linked through the damage variable and fracture strain. The governing constitutive model of Johnson-Cook [28] plasticity and progressive damage model are shown in Equations (1)–(3).

$$\sigma = (A + B \cdot \varepsilon^n) \cdot \left(1 + C \cdot ln\left(\frac{\dot{\varepsilon}}{\dot{\varepsilon_{ref}}}\right)\right) \cdot \left(1 - \left(\left(T - T_{ref}\right) / \left(T_{melt} - T_{ref}\right)\right)^m\right) \quad (1)$$

$$\varepsilon_f = \left(d_1 + d_2 \cdot e^{-d_3 \eta}\right) \cdot \left(1 + d_4 \cdot ln\left(\frac{\dot{\varepsilon}}{\dot{\varepsilon_{ref}}}\right)\right) \cdot \left(1 + d_5 \cdot \left(T - T_{ref}\right) / \left(T_{melt} - T_{ref}\right)\right) \quad (2)$$

$$D = \int \frac{d\varepsilon}{\varepsilon_f} \quad (3)$$

The model predicts the von Mises equivalent stress (σ), as a function of equivalent plastic strain (ε), plastic strain rate ($\dot{\varepsilon}$), and temperature (T), while damage is predicted with the index D, depending on the accumulative plastic strain $(d\varepsilon)$ and fracture strain $\left(\varepsilon_f\right)$. The latter depending on the stress triaxiality (η), plastic strain rate, and temperature. The fracture in the material is reached for D = 1.

The Johnson-Cook model parameters considered for sensitivity analysis include yield stress (A), hardening constant (B), hardening exponent (n), strain rate sensitivity (C), thermal sensitivity (m), and damage model constants (d_1, d_2, d_3, d_4, and d_5). The control model parameters for the blade containment simulations, listed in Table 1 [22,30], were subjected to ±5% variations to capture the model's response to small parameter fluctuations, reflecting potential uncertainties in experimental calibration. The results from these variations were compared to the control model results (using the reference parameters from Table 1), and the percentage variation was calculated to assess the impact of these fluctuations on model performance.

Table 1. Reference parameters for the J-C control model representing the plasticity and progressive damage of Ti-6Al-4V. The reference plastic strain rate, the melting temperature, and reference temperature are, respectively: $\dot{\varepsilon_{ref}}$ = 0.001, T_{melt} = 1660 °C, and T_{ref} = 25 °C [22,30].

Plasticity Related Model Constants					**Progressive Damage Model Constants**				
A (MPa)	B (MPa)	C	m	n	d_1	d_2	d_3	d_4	d_5
927.0	878.0	0.0137	0.594	0.795	0.246	186.0	−15.70	0.2582	1.206

The first full-computational model in the research literature giving qualitatively realistic results of the blade containment tests is reported in refs. [5,53]. The validation of a completely accurate model by academic research is clearly unfeasible due to the high cost of building the prototype model and the subsequent destruction under the containment test. Therefore, to reduce the uncertainty of computational results, the sensitivity analysis addressed here is a need. The aeroengine full turbofan model, analyzed within ANSYS Workbench Explicit Dynamics for sensitivity analysis of model parameters under containment testing, is given in Figure 1. Full constraints are given to the casing bores, while axial

displacement constraint is applied in the fan disk. The fan included the detached blade and rotated at a maximum testing speed of 285 rad/s [54–56] with zero initial linear velocity (Figure 1a).

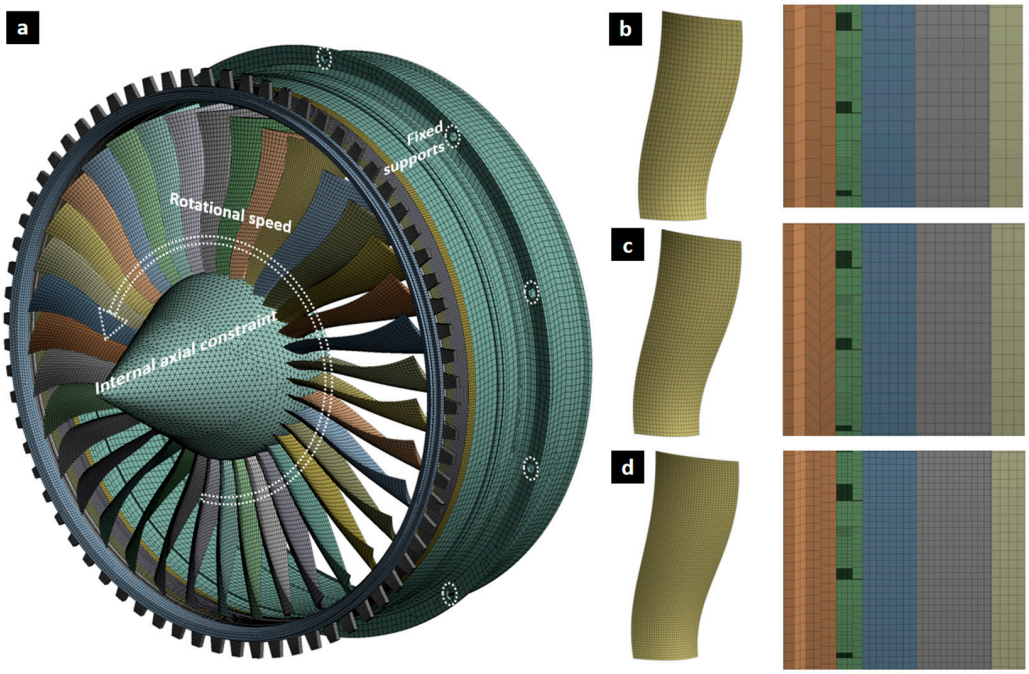

Figure 1. (**a**) Trent 1000-based turbofan model for blade-out containment simulation, showing constraints and initial conditions. Meshing details of the detached blade and the casing for (**b**) coarse, (**c**) intermediate, and (**d**) fine meshes.

A predominantly hexahedral mesh, composed primarily of SOLID164 elements, was implemented for computational efficiency and stability, particularly in regions prone to large deformations and damage (e.g., fan blades). SOLID168 tetrahedral elements were strategically incorporated only where necessary, such as in the casing ribs and other complex features, to accommodate intricate geometries while minimizing their use and mitigating potential numerical issues associated with tetrahedral formulations. The casing was divided into six axial zones, with mesh refinement applied in areas expected to experience blade impact.

To ensure numerical accuracy and computational efficiency, a mesh convergence study was performed. This involved progressively refining the model mesh and balancing the mesh density with the computational cost. Three mesh configurations were used: 168,753 nodes and 240,994 elements (Figure 1b); 244,498 nodes and 295,838 elements (Figure 1c); and 331,759 nodes and 361,035 elements (Figure 1d). Element sizes were adjusted in key areas to better capture the system's geometric and physical characteristics. The analysis aimed to identify a mesh providing an accurate representation while maintaining efficient simulation times. Refinement ceased upon achieving a suitable balance between accuracy and computational complexity.

To assess the sensitivity of the model to parameter variations, the equivalent plastic stress, damage index, and equivalent plastic strain at the last instance of impact simulation were selected as response metrics. These values, derived from turbofan simulations incorporating each parameter variation, were compared to the control model (Table 1) using relative error. The results of this sensitivity analysis are presented visually using star charts and, subsequently, ranked in order of importance.

3. Results

3.1. Mesh Convergence for Blade-Out Containment Simulation

To ensure numerical accuracy and computational efficiency, a mesh convergence study was conducted for the aeroengine blade-out containment simulation. A mesh quality assessment, using the orthogonal quality metric, yielded an average value of 0.81. This well-known metric quantifies the geometric deviation of individual elements from their ideal forms (e.g., rectangular prism or regular tetrahedron). The resultant value, approaching unity, signifies a high degree of shape conformity, suggesting the mesh's suitability to generate accurate and numerically stable simulation results [57]. A mesh convergence analysis, considering three different configurations, demonstrated proper convergence with minimal variations in the results as the mesh was refined (Figure 2). For instance, in Figure 2a, the equivalent stress in the casing impact zone varied by 7.1% between the coarse and fine meshes, and only 2.6% between the medium and fine meshes. In the detached blade (hereafter referred to as "the blade"), the variation between coarse and medium meshes was 4.8%, decreasing to 0.8% between medium and fine meshes.

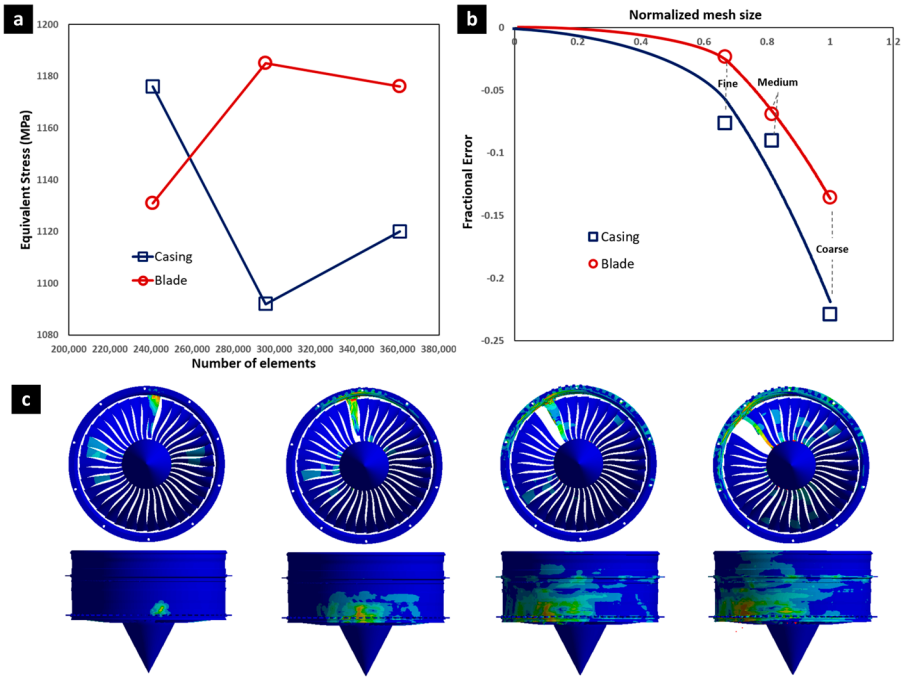

Figure 2. Convergence analysis of coarse, medium, and fine meshes of the aeroengine model for blade-out containment simulations. (**a**) Convergence of the maximum value of the equivalent stress of the fan and blades at the last simulated impact stage, with an increasing number of elements for coarse, medium, and fine meshes. (**b**) The trend of fractional error computed for the blade and casing demonstrates stagnation and convergence to zero as the normalized mesh element size decreases. (**c**) Evolution of the impact showing the detached blade and the casing deformations.

Additionally, a novel approach proposed by Tuninetti et al. [58] was employed to verify convergence through fractional error analysis, confirming that the fine mesh demonstrated convergence with negligible variation [58]. This approach verified a decreasing fractional error approaching zero with mesh refinement, confirming effective convergence (Figure 2b). Figure 2c shows the evolution of the impact, showing a detached blade and the casing deformations obtained with the refined meshed. The resulting impact dynamics and structural response of the turbofan system show nonlinear behavior characterized by rapid stress and deformation propagation in the casing and fan components. The detached blade was impacted with high energy, causing localized deformations in the casing and surround-

ing areas. Given the acceptable balance between numerical accuracy and computational cost, the fine mesh configuration was, therefore, selected for all subsequent simulations.

3.2. Aeroengine Blade-Out Containment Simulation Results Using the J-C Control Model

The blade-out containment simulation was conducted using the converged mesh and the Johnson-Cook control model parameters (Table 1). The structural response of key components, such as the detached blade, the casing, and the fan, was analyzed in terms of equivalent stress, equivalent plastic strain, and damage index. The results of the simulation are presented as contour plots in Figure 3 and summarized in Table 2, demonstrating the turbofan's capacity to contain fan blades during impact. The simulation revealed that the detached blade exhibited localized plastic deformation, reaching a maximum equivalent plastic strain of 143% and a maximum stress of 1176 MPa. The casing successfully contained the blade, experiencing significant deformation near the impact region and reaching a maximum damage index of 0.55, suggesting compromised serviceability but no critical failure. The fan blades underwent plastic strain up to 0.73, with a maximum equivalent stress of 1185 MPa and a damage index of 0.179. While the casing experienced considerable deformation near the impact area, it successfully contained the blade. The fan and remaining blades deformed within acceptable limits, without fracture. The maximum damage index of 0.51 for the casing indicates that engine service was compromised but maintained a safety factor of approximately two for damage tolerance against explosion. These observations suggest a robust structural design capable of withstanding blade-out events without compromising overall aeroengine safety, providing a solid foundation for future research or design adjustments.

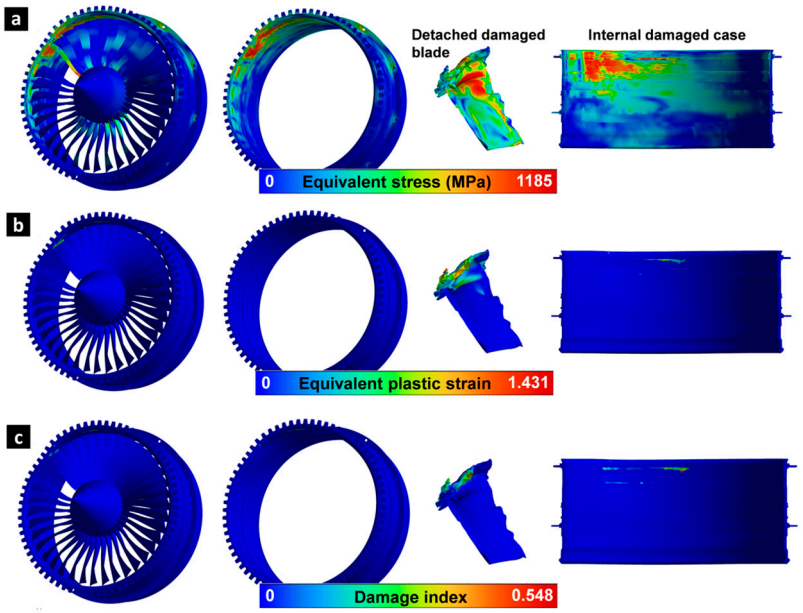

Figure 3. Summarized results of the aeroengine blade-out containment simulation: (**a**) equivalent stress; (**b**) equivalent plastic strain; (**c**) damage index.

Table 2. Maximum reached values of the equivalent strain, stress, and damage index at the last simulated stage using the control model and the selected mesh.

Component	Stress (MPa)	Plastic Strain	Damage Index
Detached blade	1176	1.431	0.548
Case	1120	1.416	0.511
Fan	1185	0.728	0.179

A sensitivity analysis is presented in the next section to ensure the result's reliability. This sensitivity analysis considers the specific ranges of plastic strain rate, equivalent plastic strain, temperature, and stress triaxiality observed at critical points in the blade and the casing during a simulated blade detachment event under operational conditions. These ranges are plastic strain rate—0 to 1.2×10^4 s^{-1} (blade) and 0 to 1.1×10^4 s^{-1} (casing); temperature—25 °C to 700 °C (blade) and 25 °C to 400 °C (casing); and stress triaxiality——−0.6 to 0.5 (blade) and −2.7 to 0.7 (casing).

3.3. Influence of J-C Parameter Variation on Plasticity in a Aeroengine Blade-Out Scenario

Numerical simulations of a fan blade-out event in a full aeroengine model were conducted to assess the influence of Johnson-Cook plasticity parameters (*A*, *B*, *n*, *C*, and *m*) on equivalent stress and equivalent plastic strain at the last stage of the simulation. Each parameter was varied by ±5%, and the resulting percentage changes in stress and strain were recorded. The relative error between the results from the control model and the model with variations was calculated and presented in star plots to visualize the sensitivity of plasticity model parameters on the plastic stress and strain response (Figure 4). These observed changes in simulation results arise from the complex interplay between component impact interactions and altered stress/strain distributions due to variations in Johnson-Cook model parameters. In addition, the complex geometry leads to nonlinear interactions between the large deformations of the blade and the casing, making a precise explanation and quantification of parameter sensitivity challenging. While general trends are discernible (e.g., increasing *A* elevates stress), accurately determining the magnitude of these effects necessitates detailed simulations such as those presented here.

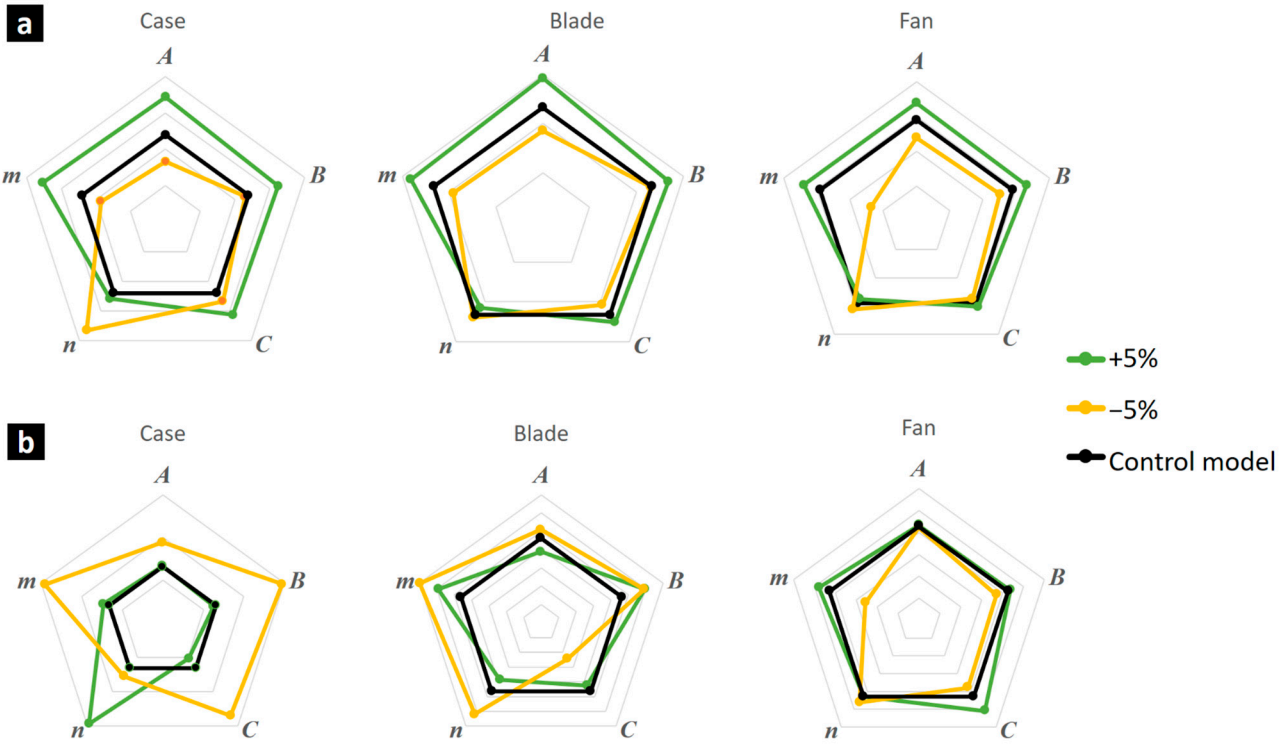

Figure 4. Star plots illustrating the sensitivity of the plasticity model parameters on the resulting plastic strain response: (**a**) equivalent stress; (**b**) equivalent plastic strain.

Analyzing the simulation results for parameter *A*, a 5% increase caused a general stress increase in all components, most notably in the case (4.58%). Strain changes were minimal. Conversely, a 5% decrease in *A* led to a stress reduction, with the largest decrease in the

case (−3.26%). However, strain increased in the case (2.03%). These trends are explained by the nature of the material behavior and the resulting identified J-C model. Increasing the initial yield strength (A) directly elevates material strength, leading to higher stresses. Consequently, a stronger case (higher A) requires less strain to absorb the impact energy.

Parameters B and n govern strain hardening. Increasing either results in larger stress, increases strain, and potentially lowers strain accumulation, particularly in the case. This was observed when a 5% increase in B caused a stress increase in the case of 3.79%, and in the fan, it caused a stress increase of 1.73%. Strain showed a negative variation in the case (−0.2%) and increases in both the blade (4.62%) and the fan (1.33%). This increase may be explained by the fact that the casing becomes more rigid, forcing the blades to deform at a higher level. Decreasing B resulted in slight stress reductions across all components, with the case experiencing the largest decrease (−0.45%). The strain in the case, as expected, increased by 5.76%. In the variations in the hardening coefficient n, the 5% increase also produced higher stress in all components, as expected: 0.85% in the case and 0.6% in the fan. Decreasing n by 5% resulted in a stress increase in the case of 5.66%, along with minimal increases in the blade (0.33%) and in the fan (0.93%). This could be attributed to the higher localized impact, as the blade became stronger, producing a higher deformation in the case, and, consequently, higher stress than the effect of decreasing n. Strain increased in all components when decreasing n; 5.42% in the blade and 4.60% in the fan, with a lower effect in the case (0.85%).

Regarding m, a 5% increase led to increases in stress and strain, which were most pronounced in the case (which had a 5.01% stress increase and a 0.51% strain increase) and the blade (which had a 2.06% stress increase), along with a strain increase in the fan (7.12%). A 5% decrease in m caused stress to decrease in all components, most noticeably in the fan (−6.51%), while strain increased in the case (5.64%) and the blade (8.21%), and decreased significantly in the fan (−23.52%). Increasing the thermal softening exponent (m) clearly reduces strength at higher temperatures. Given the constant impact energy, which was absorbed as plastic energy and the consequent temperature increase in the softened material, the blade especially reached a higher level of plastic deformation compared to the case in all simulations, and, consequently, higher softening due to the m variation. This increases its sensitivity, exhibiting higher plastic strain during the impact.

Elevating the strain rate factor (C) strengthens the material, increasing stress, and localizing deformations. The 5% increase in C increased stress in the case, as expected, by 3.28% and, to a lesser extent, the blade by 0.78% and the fan by 0.46%. The strain decreased by −0.97% in the case, and in the blade, it decreased by −1.24% but increased significantly in the fan by 11.62%. Reducing C by 5% yielded mixed results for stress and strain. Case stress increased by 1.21%, while blade and fan stress decreased by −1.08% and −0.68%, respectively. The strain increased by 4.88% in the case, possibly due to the more localized impact; as in the blade it decreased by −7.61%, and in the fan, it decreased by −6.43%.

3.4. Influence of J-C Parameter Variation on Damage Evolution of Aeroengine Blade-Out

The sensitivity analysis assessing the impact of ±5% variations in Johnson-Cook parameters on damage in aeroengine components is shown in Figure 5 in two groups: plasticity model and damage model parameters. The results reveal that a 5% increase in parameter A caused a considerable damage increase in the casing (+15.48%), and minor increases in the blade (+3.4%) and fan (+0.73%). A 5% decrease drastically reduced damage in the casing (−28.28%) and the blade (−30.15%), slightly increasing fan damage (+5.63%). Parameter B, with the 5% increase, significantly increased fan damage (+10.34%), while reducing casing (−18.22%) and blade damage (−30.79%). Decreasing B had mixed effects, reducing casing damage (−17.79%) but significantly increasing blade damage (+60.79%).

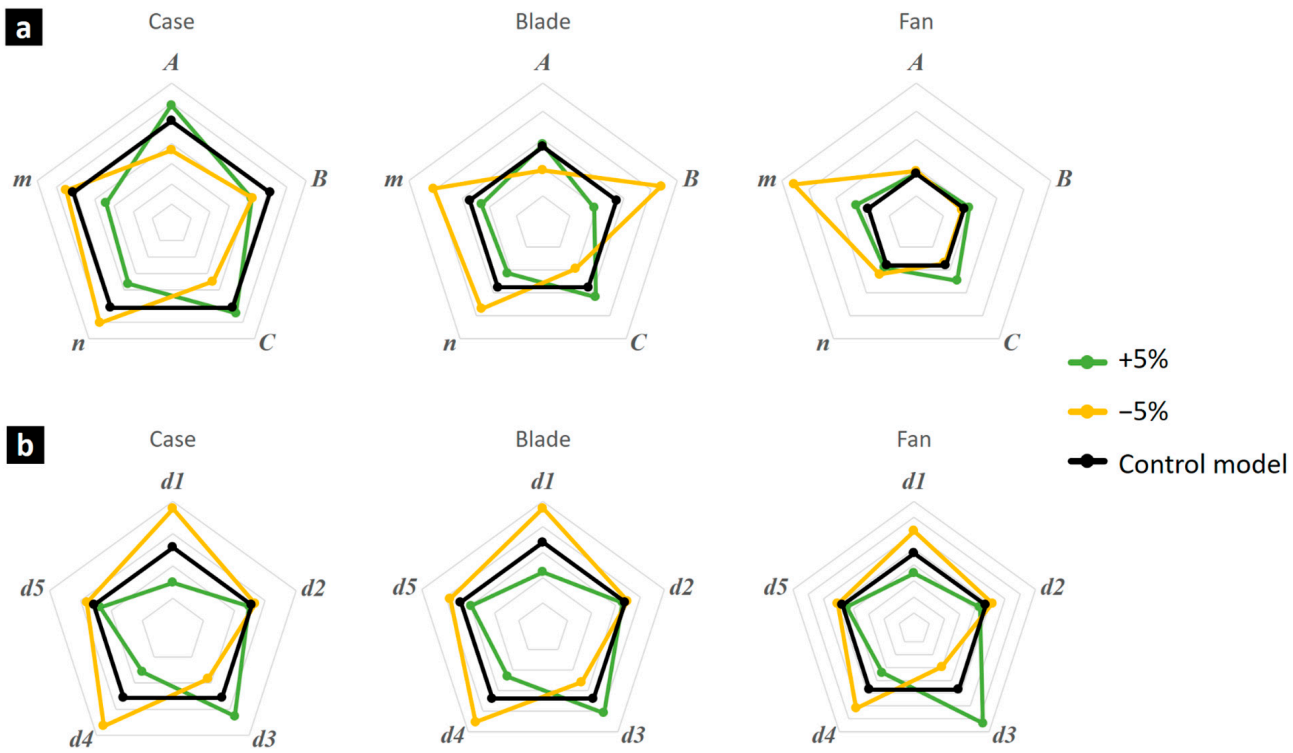

Figure 5. Sensitivity of (**a**) plasticity and (**b**) damage model parameters on the damage (index) response of casing, the fan, and the detached blade.

Increasing C increased damage across all components, most notably in the fan (+38.08%). A 5% decrease substantially reduced casing (−31.43%) and blade damage (−28.64%).

In total, the 5% increase in both n (hardening coefficient) and m (thermal coefficient) significantly reduced casing and blade damage. Decreasing n increased blade and fan damage, while decreasing m, which substantially increased damage across all components, especially in the fan (+155.27%).

For the damage model parameters ($d1$–$d5$), $d1$ had the most pronounced effect on damage across all components, while $d2$ had the lowest effect. Parameter $d3$ strongly influenced fan damage, $d4$ caused similar changes across all components, and $d5$ had a minimal impact.

Figure 6 shows the influence of deterministic Johnson-Cook plasticity and damage model parameters on the damage index in order, from most influential to less influential in the fan, casing, and the blade (detached blade). Note that decreasing the thermal softening exponent (m) had a disproportionately large impact on fan damage. Because the initial damage index in the fan obtained with the J-C control model was very low (0.179), any increase appears as a large percentage change, even if the absolute change is relatively small. A 5% decrease in m accelerates thermal softening, leading to more extensive damage propagation in the fan during the blade-out event. While a 155.27% increase sounds dramatic, it represents an absolute increase of only 0.093 in the damage index. This seemingly small change is significant because the damage obtained from the control model is so low. Essentially, the sensitivity is amplified by the low initial value.

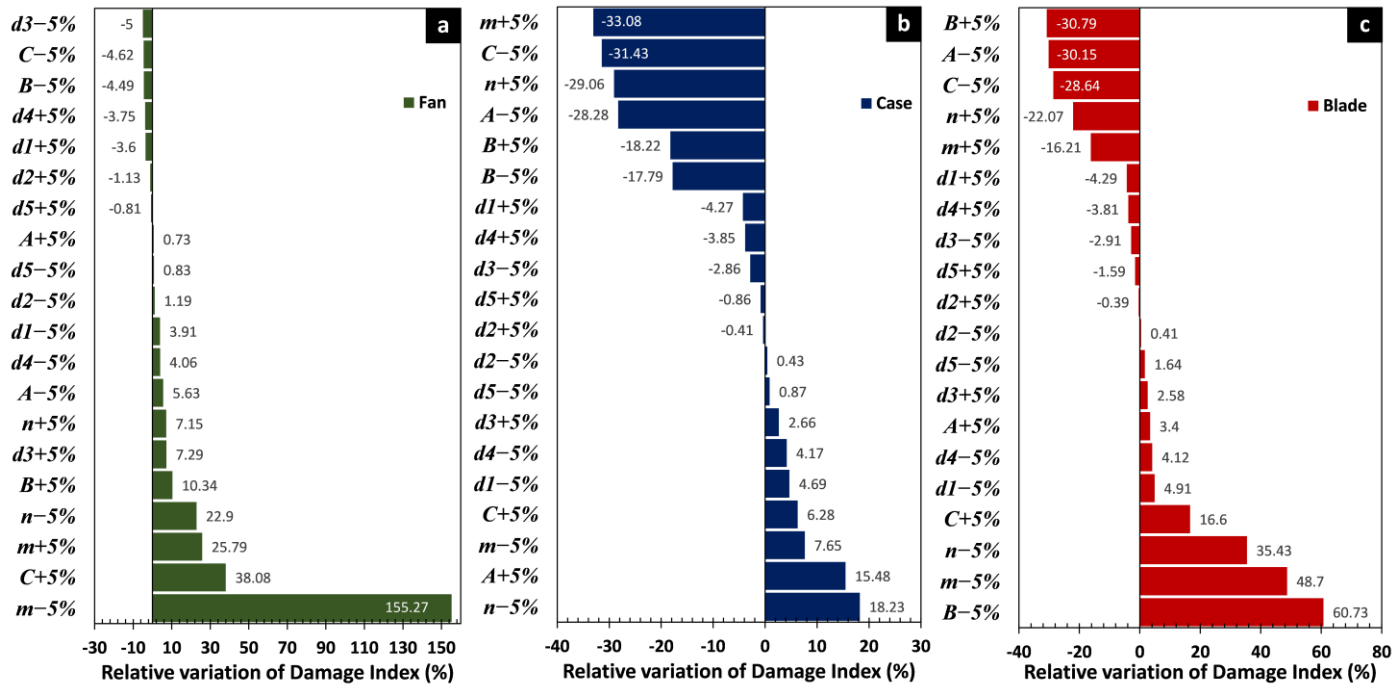

Figure 6. Order or influence of deterministic Johnson-Cook plasticity and damage model parameters on the damage index of the (**a**) fan, (**b**) the casing, and (**c**) the detached blade during a fan blade-out event of aircraft engine.

While fan damage is a major concern, the integrity of the casing is most critical to the safety of the aircraft, acting as the primary containment barrier during a blade-out or other engine failure event. In this critical component, the thermal coefficient (m) also had the largest influence on damage ($\pm$33%), followed by the strain rate hardening coefficient (C), and the strain hardening exponent (n), yield strength (A), and parameter B. Parameter $d1$ exhibited the most substantial effect on damage prediction; a 5% increase in $d1$ resulted in a decrease in predicted damage, while a 5% decrease led to an increase. Conversely, $d2$ demonstrated a minimal impact on damage (around $\pm$0.4%). The parameters $d4$, $d3$, and $d5$ followed $d1$ in order of influence on both the case and the detached blade damage.

4. Conclusions

This study conducted a comprehensive local sensitivity analysis of the Johnson-Cook plasticity and the progressive damage model for Ti-6Al-4V titanium alloy, a crucial material constituting 14% of modern aircraft weight, and which is commonly used in aeroengine components. The analysis focused on identifying the most influential JC parameters affecting the predicted structural response of these components during a blade-out event. A preliminary mesh convergence study, using a fine mesh with an average orthogonal quality of 0.81, ensured the accuracy and reliability of the subsequent sensitivity analysis. The convergence study demonstrated an acceptable convergence of the maximum equivalent stress in both the casing impact zone (2.6% difference between medium and fine meshes) and the blade (0.8% difference between medium and fine meshes). A fractional error approach further validated the observed convergence.

The blade-out containment simulation, performed with the converged mesh, revealed key aspects of the structural behavior:

- Nonlinear behavior during blade detachment, characterized by rapid stress and deformation propagation, localized casing deformation due to the high-energy blade

impact, and the maximum equivalent plastic strain of 143% in the detached blade, 142% in the casing, and 73% in the fan.

- A maximum damage index of 0.55 in the casing, indicating potential damage but below critical failure levels for affecting the structural integrity of the aircraft.

The sensitivity analysis, involving ±5% variations in JC parameters, revealed the following:

- A strong dependence of damage predictions on specific model parameters, particularly the thermal softening coefficient (m). Variations in m resulted in ±33% changes in casing damage, highlighting its critical role in accurate damage prediction.
- Other influential parameters, in decreasing order of importance, include the strain rate hardening coefficient (C), the strain hardening exponent (n), and yield strength (A). Parameters B, $d1$, $d4$, and $d3$ exhibited moderate to minor influence, while $d5$ and $d2$ showed a minimal impact on casing damage.

This work underscores the importance of precisely calibrating JC model parameters, especially m, for reliable assessments of aeroengine casing integrity during blade-out events. The identified sensitivities provide essential data for robust design and safety evaluations of aeroengine components. This local sensitivity analysis highlights the individual influence of Johnson-Cook model parameters. To further improve the accuracy and reliability of damage predictions in aeroengine applications, future research should investigate global sensitivity analyses that consider parameter interactions. Additionally, the coupled effects of temperature and strain rate, which are not captured by the standard J-C model, should be explored using modified models. This would provide a more comprehensive understanding of the model's behavior and contribute to improved safety and performance in aeroengine design.

Author Contributions: Conceptualization, C.B. and V.T.; methodology, C.B., H.S. and V.T.; software, C.B. and H.S.; validation, C.B., G.P. and V.T.; formal analysis, C.B., L.D., A.M.H., A.O. and V.T.; investigation, C.B., H.S., A.O. and V.T.; resources, A.M.H. and V.T.; data curation, C.B., H.S. and V.T.; writing—original draft preparation, C.B. and V.T.; writing—review and editing, C.B., G.P., A.M.H., L.D., A.O. and V.T.; visualization, C.B. and V.T.; supervision, V.T.; project administration, V.T.; funding acquisition, V.T. All authors have read and agreed to the published version of the manuscript.

Funding: This research received no external funding.

Data Availability Statement: The original contributions presented in this study are included in the article. Further inquiries can be directed to the corresponding author.

Conflicts of Interest: The authors declare no conflicts of interest.

References

1. Mosallanejad, M.H.; Abdi, A.; Karpasand, F.; Nassiri, N.; Iuliano, L.; Saboori, A. Additive Manufacturing of Titanium Alloys: Processability, Properties, and Applications. *Adv. Eng. Mater.* **2023**, *25*, 2301122. [CrossRef]
2. del Bosque, A.; Fernández-Arias, P.; Vergara, D. Titanium Additive Manufacturing with Powder Bed Fusion: A Bibliometric Perspective. *Appl. Sci.* **2024**, *14*, 10543. [CrossRef]
3. Fernandes, F.A.O.; Gonçalves, J.J.M.; Pereira, A.B. Evaluation of Laser Lap Weldability between the Titanium Alloy Ti-6Al-4V and Aluminum Alloy 6060-T6. *Crystals* **2023**, *13*, 1448. [CrossRef]
4. Tuninetti, V.; Oñate, A.; Valenzuela, M.; Sepúlveda, H.; Pincheira, G.; Medina, C.; García-Herrera, C.; Duchêne, L.; Habraken, A.M. Characterization Approaches Affect Asymmetric Load Predictions of Hexagonal Close-Packed Alloy. *J. Mater. Res. Technol.* **2023**, *26*, 5028–5036. [CrossRef]
5. Tuninetti, V.; Sepúlveda, H. Computational Mechanics for Turbofan Engine Blade Containment Testing: Fan Case Design and Blade Impact Dynamics by Finite Element Simulations. *Aerospace* **2024**, *11*, 333. [CrossRef]

6. Cui, C.; Hu, B.M.; Zhao, L.; Liu, S. Titanium Alloy Production Technology, Market Prospects and Industry Development. *Mater. Des.* **2011**, *32*, 1684–1691. [CrossRef]
7. Rajendran, R.; Venkateshwarlu, M.; Petley, V.; Verma, S. Strain Hardening Exponents and Strength Coefficients for Aeroengine Isotropic Metallic Materials—A Reverse Engineering Approach. *J. Mech. Behav. Mater.* **2014**, *23*, 101–106. [CrossRef]
8. Miko, T.; Petho, D.; Gergely, G.; Markatos, D.; Gacsi, Z. A Novel Process to Produce Ti Parts from Powder Metallurgy with Advanced Properties for Aeronautical Applications. *Aerospace* **2023**, *10*, 332. [CrossRef]
9. Inagaki, I.; Takechi, T.; Shirai, Y.; Ariyasu, N. Application and Features of Titanium for the Aerospace Industry. *Nippon Steel Sumitomo Met. Tech.* **2014**, *106*, 22–27.
10. Vijayaraghavan, V.; Castagne, S. Measurement of Surface Characteristics of Ti6Al4V Aerospace Engineering Components in Mass Finishing Process. *Meas. J. Int. Meas. Confed.* **2018**, *115*, 279–287. [CrossRef]
11. Carney, K.S.; Pereira, J.M.; Revilock, D.M.; Matheny, P. Jet Engine Fan Blade Containment Using an Alternate Geometry. *Int. J. Impact Eng.* **2009**, *36*, 720–728. [CrossRef]
12. Sinha, S.K.; Dorbala, S. Dynamic Loads in the Fan Containment Structure of a Turbofan Engine. *J. Aerosp. Eng.* **2008**, *323*, 1–14. [CrossRef]
13. Buzyurkin, A.E.; Gladky, I.L.; Kraus, E.I. Determination of Parameters of the Johnson-Cook Model for the Description of Deformation and Fracture of Titanium Alloys. *J. Appl. Mech. Tech. Phys.* **2015**, *56*, 330–336. [CrossRef]
14. Mangal, S.; Kambhammettu, S.K.S.; Rao, C.L. Oblique Impact Simulation Study of Ti-6Al-4 V Alloy Plates for Analysis of Blade-Off Event in Turbofan Aero-Engine. In *Dynamic Behavior of Soft and Hard Materials Volume 1*; Velmurugan, R., Balaganesan, G., Kakur, N., Kanny, K., Eds.; Springer Nature: Singapore, 2024; pp. 365–379.
15. Holenko, K.; Koda, E.; Kernytskyy, I.; Babak, O.; Horbay, O.; Popovych, V.; Chalecki, M.; Leśniewska, A.; Berezovetskyi, S.; Humeniuk, R. Evaluation of Accelerator Pedal Strength under Critical Loads Using the Finite Element Method. *Appl. Sci.* **2023**, *13*, 6684. [CrossRef]
16. Cortis, G.; Nalli, F.; Sasso, M.; Cortese, L.; Mancini, E. Effects of Temperature and Strain Rate on the Ductility of an API X65 Grade Steel. *Appl. Sci.* **2022**, *12*, 2444. [CrossRef]
17. Jiang, X.; Ding, J.; Wang, C.; Shiju, E.; Hong, L.; Yao, W.; Wang, H.; Zhou, C.; Yu, W. Parameter Identification of Johnson–Cook Constitutive Model Based on Genetic Algorithm and Simulation Analysis for 304 Stainless Steel. *Sci. Rep.* **2024**, *14*, 21221. [CrossRef] [PubMed]
18. Khare, S.; Kumar, K.; Choudhary, S.; Singh, P.K.; Verma, R.K.; Mahajan, P. Determination of Johnson–Cook Material Parameters for Armour Plate Using DIC and FEM. *Met. Mater. Int.* **2021**, *27*, 4984–4995. [CrossRef]
19. Osorio-Pinzon, J.C.; Abolghasem, S.; Casas-Rodriguez, J.P. Predicting the Johnson Cook Constitutive Model Constants Using Temperature Rise Distribution in Plane Strain Machining. *Int. J. Adv. Manuf. Technol.* **2019**, *105*, 279–294. [CrossRef]
20. Yin, W.; Liu, Y.; He, X.; Tian, Z. Parametric Analysis and Improvement of the Johnson-Cook Model for a TC4 Titanium Alloy. *Metals* **2024**, *14*, 1199. [CrossRef]
21. Sambo, A.M.; Younas, M.; Njuguna, J. Insights into Machining Techniques for Additively Manufactured Ti6Al4V Alloy: A Comprehensive Review. *Appl. Sci.* **2024**, *14*, 10340. [CrossRef]
22. Tuninetti, V.; Sepúlveda, H.; Beecher, C.; Rojas-Ulloa, C.; Oñate, A.; Medina, C.; Valenzuela, M. A Combined Experimental and Numerical Calibration Approach for Modeling the Performance of Aerospace-Grade Titanium Alloy Products. *Aerospace* **2024**, *11*, 285. [CrossRef]
23. Yin, W.; Liu, Y.; He, X.; Li, H. Effects of Different Materials on Residual Stress Fields of Blade Damaged by Foreign Objects. *Materials* **2023**, *16*, 3662. [CrossRef]
24. Rodríguez Prieto, J.M.; Larsson, S.; Afrasiabi, M. Thermomechanical Simulation of Orthogonal Metal Cutting with PFEM and SPH Using a Temperature-Dependent Friction Coefficient: A Comparative Study. *Materials* **2023**, *16*, 3702. [CrossRef] [PubMed]
25. Zhao, Z.; Ji, H.; Zhong, Y.; Han, C.; Tang, X. Mechanical Properties and Fracture Behavior of a TC4 Titanium Alloy Sheet. *Materials* **2022**, *15*, 8589. [CrossRef]
26. Zhao, Z.; Wang, L.; Zhang, J.; Liu, L.; Chen, W. Prediction of High-Cycle Fatigue Strength in a Ti-17 Alloy Blade after Foreign Object Damage. *Eng. Fract. Mech.* **2021**, *241*, 107385. [CrossRef]
27. Shi, L.; Wang, T.; Wang, L.; Liu, E. Research on Johnson–Cook Constitutive Model of γ-TiAl Alloy with Improved Parameters. *Materials* **2023**, *16*, 6715. [CrossRef] [PubMed]
28. Johnson, G.R.; Cook, W.H. Fracture Characteristics of Three Metals Subjected to Various Strains, Strain Rates, Temperatures and Pressures. *Eng. Fract. Mech.* **1985**, *21*, 31–48. [CrossRef]
29. Johnson, G.R.; Cook, W.H. A Constitutive Model and Data for Metals Subjected to Large Strains, High Strain Rates and High Temperatures. In Proceedings of the 7th International Symposium on Ballistics, The Hague, The Netherlands, 19–21 April 1983; pp. 541–547.

30. Tuninetti, V.; Forcael, D.; Valenzuela, M.; Martínez, A.; Ávila, A.; Medina, C.; Pincheira, G.; Salas, A.; Oñate, A.; Duchêne, L. Assessing Feed-Forward Backpropagation Artificial Neural Networks for Strain-Rate-Sensitive Mechanical Modeling. *Materials* **2024**, *17*, 317. [CrossRef] [PubMed]
31. He, Q.; Xuan, H.J.; Liao, L.F.; Hong, W.R.; Wu, R.R. Simulation Methodology Development for Rotating Blade Containment Analysis. *J. Zhejiang Univ. Sci. A* **2012**, *13*, 239–259. [CrossRef]
32. Bai, C.; Xuan, H.; Huang, X.; He, Z.; Hong, W. Containment Ability and Groove Depth Design of U Type Protection Ring. *Chin. J. Aeronaut.* **2016**, *29*, 395–402. [CrossRef]
33. Wimperis, H.E. The Future of Flying. *Nature* **1939**, *144*, 538–541. [CrossRef]
34. Choi, Y.; Lee, J. Estimation of Liquid Hydrogen Fuels in Aviation. *Aerospace* **2022**, *9*, 564. [CrossRef]
35. Faure, A.; Schuermans, B.; Wang, G.; Caruso, S.; Zahn, M.; Noiray, N. Acoustic Transfer Matrix of High-Pressure Hydrogen/Air Flames for Aircraft Propulsion. *Combust. Flame* **2024**, *270*, 113776. [CrossRef]
36. Ruffles, P.C. Aero Engines of the Future. *Aeronaut. J.* **2003**, *107*, 307–322. [CrossRef]
37. Pollock, T.M. Alloy Design for Aircraft Engines. *Nat. Mater.* **2016**, *15*, 809–815. [CrossRef] [PubMed]
38. Tirpak, J.A. Next-Gen Fighter Engines. *Air Force Mag.* **2023**, *106*, 42–45.
39. Ye, D.; Xuan, H.J.; Liu, L.L. Research Overview of Full Aero-Engine Dynamic Response Caused by Blade-Off. *Appl. Mech. Mater.* **2013**, *423–426*, 1552–1557. [CrossRef]
40. Yu, P.; Zhang, D.; Ma, Y.; Hong, J. Dynamic Modeling and Vibration Characteristics Analysis of the Aero-Engine Dual-Rotor System with Fan Blade Out. *Mech. Syst. Signal Process.* **2018**, *106*, 158–175. [CrossRef]
41. He, Q.; Xie, Z.; Xuan, H.; Liu, L.; Hong, W. Multi-Blade Effects on Aero-Engine Blade Containment. *Aerosp. Sci. Technol.* **2016**, *49*, 101–111. [CrossRef]
42. He, Q.; Xie, Z.; Xuan, H.; Hong, W. Ballistic Testing and Theoretical Analysis for Perforation Mechanism of the Fan Casing and Fragmentation of the Released Blade. *Int. J. Impact Eng.* **2016**, *91*, 80–93. [CrossRef]
43. Roy, P.A.; Meguid, S.A. Containment of Blade Shedding in Gas Turbine Engines: Part II—Experimental and Numerical Investigations. *Int. J. Mech. Mater. Des.* **2021**, *17*, 13–24. [CrossRef]
44. Cendón, D.A.; Erice, B.; Gálvez, F.; Sánchez-Gálvez, V. Numerical Simulation of Tangling in Jet Engine Turbines. *Int. J. Turbo Jet Engines* **2012**, *29*, 269–282. [CrossRef]
45. Saltelli, A.; Tarantola, S.; Campolongo, F.; Ratto, M. Sensitivity Analysis in Practice: A Guide to Assessing Scientific Models. In *Sensitivity Analysis in Practice: A Guide to Assessing Scientific Models*; John Wiley & Sons, Ltd.: Hoboken, NJ, USA, 2002; ISBN 9780470870952.
46. Torii, A.J.; Novotny, A.A. A Priori Error Estimates for Local Reliability-Based Sensitivity Analysis with Monte Carlo Simulation. *Reliab. Eng. Syst. Saf.* **2021**, *213*, 107749. [CrossRef]
47. Jardin, R.T.; Tuninetti, V.; Tchuindjang, J.T.; Hashemi, N.; Carrus, R.; Mertens, A.; Duchêne, L.; Tran, H.S.; Habraken, A.M. Sensitivity Analysis in the Modelling of a High Speed Steel Thin-Wall Produced by Directed Energy Deposition. *Metals* **2020**, *10*, 1554. [CrossRef]
48. Teixeira, R.; O'Connor, A.; Nogal, M. Probabilistic Sensitivity Analysis of Offshore Wind Turbines Using a Transformed Kullback-Leibler Divergence. *Struct. Saf.* **2019**, *81*, 101860. [CrossRef]
49. Gallo, C.; Duchêne, L.; Quy Duc Pham, T.; Jardin, R.; Tuninetti, V.; Habraken, A.-M. Impact of Boundary Parameters Accuracy on Modeling of Directed Energy Deposition Thermal Field. *Metals* **2024**, *14*, 173. [CrossRef]
50. Razavi, S.; Jakeman, A.; Saltelli, A.; Prieur, C.; Iooss, B.; Borgonovo, E.; Plischke, E.; Lo Piano, S.; Iwanaga, T.; Becker, W.; et al. The Future of Sensitivity Analysis: An Essential Discipline for Systems Modeling and Policy Support. *Environ. Model. Softw.* **2021**, *137*, 104954. [CrossRef]
51. Tuninetti, V.; Habraken, A.M. Impact of Anisotropy and Viscosity to Model the Mechanical Behavior of Ti-6Al-4V Alloy. *Mater. Sci. Eng. A* **2014**, *605*, 39–50. [CrossRef]
52. Tuninetti, V.; Flores, P.; Valenzuela, M.; Pincheira, G.; Medina, C.; Duchêne, L.; Habraken, A.M. Experimental Characterization of the Compressive Mechanical Behaviour of Ti6Al4V Alloy at Constant Strain Rates over the Full Elastoplastic Range. *Int. J. Mater. Form.* **2020**, *13*, 709–724. [CrossRef]
53. Sepúlveda, H.; Valle, R.; Pincheira, G.; Prasad, C.S.; Salas, A.; Medina, C.; Tuninetti, V. Dynamic Numerical Prediction of Plasticity and Damage in a Turbofan Blade Containment Test. *Proc. Inst. Mech. Eng. Part L J. Mater. Des. Appl.* **2023**, *237*, 2551–2560. [CrossRef]
54. EASA. *Type-Certificate Data Sheet: Trent 1000 Series*; EASA: Blankenfelde-Mahlow, Germany, 2024.
55. Yang, B. Blade Containment Evaluation of Civil Aircraft Engines. *Chin. J. Aeronaut.* **2013**, *26*, 9–16. [CrossRef]
56. FAA (Federal Aviation Administration). 14-Aeronautics and Space, 14 CFR § 33.94—Blade Containment and Rotor Unbalance Tests. Code of Federal Regulations (Annual Edition). 2016. Available online: https://www.govinfo.gov/content/pkg/CFR-2016-title14-vol1/pdf/CFR-2016-title14-vol1-chapI.pdf (accessed on 12 December 2024).

57. ANSYS Inc. *ANSYS Meshing User's Guide*; ANSYS Inc.: Canonsburg, PA, USA, 2010; Volume 13, pp. 1–342.
58. Tuninetti, V.; Gómez, Á.; Bustos, F.; Oñate, A.; Hinojosa, J.; Gallo, C.; Habraken, A.; Duchêne, L. Computational Modeling of U-Shaped Seismic Dampers for Structural Damage Mitigation. *Appl. Sci.* **2024**, *14*, 10238. [CrossRef]